Abbreviations

amyotrophic lateral sclerosis (ALS)
alpha-amino-3-hydroxy-5-methyl-4-isoxazolepropionic acid (AMPA)
adaptor protein-4 (AP-4)
EGF receptor (EGFR)
Huntington's disease (HD)
N-methyl-4-phenyl-1,2,3,6-tetrahydropyridine (MPTP)
mammalian target of rapamycin (mTOR)
Parkinson's disease (PD)
progressive motor neuronopathy (*pmn*)
transmembrane AMPA receptor regulatory protein (TARP)
leucine-rich repeat Ig-containing protein (LINGO-1)
Wallerian degeneration slow (*Wlds*)

References

1. Palop JJ, Chin J, Mucke L (2006) A network dysfunction perspective on neurodegenerative diseases. Nature 443:768–773
2. Yamamoto A, Lucas JJ, Hen R (2000) Reversal of neuropathology and motor dysfunction in a conditional model of Huntington's disease. Cell 101:57–66
3. Orr HT, Zoghbi HY. (2000) Reversing neurodegeneration: a promise unfolds. Cell 101:1–4
4. Wang J, Wang C-E, Orr A, Tydlacka S, Li S-H, Li X-J (2008) Impaired ubiquitin – proteasome system activity in the synapses of Huntington's disease mice. J Cell Biol 180:1177–1189
5. Eberhardt O,Coelln RV, Kugler S, Lindenau J, Rathke-Hartlieb S, Gerhardt E, Haid S, Isenmann S, Gravel C, Srinivasan A et al. (2000) Protection by synergistic effects of adenovirus-mediated X chromosome-linked inhibitor of apoptosis and glial cell line-derived neurotrophic factor gene transfer in the 1-methyl-4-phenyl-1,2,3,6-tetrahydropyridine model of Parkinson's disease. J Neurosci 20:9126–9134
6. Vila M, Jackson-Lewis V, Vukosavic S, Djaldetti R, Liberatore G, Offen D, Korsmeyer SJ, Przedborski S (2001) Bax ablation prevents dopaminergic neurodegeneration in the 1-methyl-4-phenyl-1,2,3,6-tetrahydropyridine mouse model of Parkinson's disease. Proc Natl Acad Sci USA 98:2837–2842
7. Inoue H, Tsukita K, Iwasato T, Suzuki Y, Tomioka M, Tateno M, Nagao M, Kawata A, Saido TC, Miura M et al. (2003) The crucial role of caspase-9 in the disease progression of a transgenic ALS mouse model. EMBO J 22:6665–6674
8. Gould TW, Buss RR, Vinsant S, Prevette D, Sun W, Knudson CM, Milligan CE, Oppenheim (2006) Complete dissociation of motor neuron death from motor dysfunction by Bax deletion in a mouse model of ALS. J Neurosci 26:8774–8786
9. Fischer LR, Glass JD (2007) Axonal degeneration in motor neuron disease. Neurodegener Dis 4:431–442
10. Sagot Y, Vejsada R, Kato A (1997) Clinical and molecular aspects of motoneurone diseases: animal models, neurotrophic factors and Bcl-2 oncoprotein. Trends Pharmacol Sci 18:330–337
11. Finn JT, Weil M, Archer F, Siman R, Srinivasan A, Raff MC (2000) Evidence that Wallerian degeneration and localized axon degeneration induced by local neurotrophin deprivation do not involve caspases. J Neurosci 20:1333–1341
12. Orimo S, Uchihara T, Nakamura A, Mori F, Kakita A, Wakabayashi K, Takahashi H (2008) Axonal α-synuclein aggregates herald centripetal degeneration of cardiac sympathetic nerve in Parkinson's disease. Brain 131:642–650

UNCORRECTED PROOF

13. Bradley WG, Good P, Rasool CG, Adelman LS (1983) Morphometric and biochemical studies of peripheral nerves in amyotrophic lateral sclerosis. Ann Neurol 14:267–277
14. Fischer LR, Culver DG, Tennant P, Davis AA, Wang M, Castellano-Sanchez A, Khan J, Polak MA, Glass JD (2004) Amyotrophic lateral sclerosis is a distal axonopathy: evidence in mice and man. Exp Neurol 185:232–240
15. Kanai K, Kuwabara S, Misawa S, Tamura N, Ogawara K, Nakata M, Sawai S, Hattori T, Bostock H (2006) Altered axonal excitability properties in amyotrophic lateral sclerosis: impaired potassium channel function related to disease stage. Brain 129:953–962
16. Vucic S, Kiernan MC (2006) Axonal excitability properties in amyotrophic lateral sclerosis. Clin Neurophysiol 117:1458–1466
17. Nakata M, Kuwabara S, Kanai K, Misawa S, Tamura N, Sawai S, Hattori T, Bostock H (2006) Distal excitability changes in motor axons in amyotrophic lateral sclerosis. Clin Neurophysiol 117:1444–1448
18. Pasinelli P, Brown RH (2006) Molecular biology of amyotrophic lateral sclerosis: insights from genetics. Nat Rev Neurosci 7:710–723
19. Coleman M (2005) Axon degeneration mechanisms: commonality amid diversity. Nat Rev Neurosci 6:889–898
20. Hara T, Nakamura K, Matsui M, Yamamoto A, Nakahara Y, Suzuki-Migishima R, Yokoyama M, Mishima K, Saito I, Okano H et al. (2006) Suppression of basal autophagy in neural cells causes neurodegenerative disease in mice. Nature 441:885–889
21. Komatsu M, Waguri S, Chiba T, Murata S, Iwata J, Tanida I, Ueno T, Koike M, Uchiyama Y, Kominami E et al. (2006) Loss of autophagy in the central nervous system causes neurodegeneration in mice. Nature 441:880–884
22. Komatsu M, Wang QJ, Holstein GR, Friedrich VL Jr, Iwata J, Kominami E, Chait BT, Tanaka K, Yue Z. (2007) Essential role for autophagy protein Atg7 in the maintenance of axonal homeostasis and the prevention of axonal degeneration. Proc Natl Acad Sci USA 104: 14489–14494
23. Mizushima N, Levine B, Cuervo AM, Klionsky DJ (2008) Autophagy fights disease through cellular self-digestion. Nature 451:1069–1075
24. Komatsu M, Waguri S, Koike M, Sou Y, Ueno T, Hara T, Mizushima N, Iwata J, Ezaki J, Murata S et al. (2007) Homeostatic levels of p62 control cytoplasmic inclusion body formation in autophagy-deficient mice. Cell 131:1149–1163
25. Matsuda S, Miura E, Matsuda K, Kakegawa W, Kohda K, Watanabe M, Yuzaki M (2008) Accumulation of AMPA receptors in autophagosomes in neuronal axons lacking adaptor protein AP-4. Neuron 57:730–745
26. Inoue H, Lin L, Lee X, Shao Z, Mendes S, Snodgrass-Belt P, Sweigard H, Engber T, Pepinsky B, Yang L et al. (2007) Inhibition of the leucine-rich repeat protein LINGO-1 enhances survival, structure, and function of dopaminergic neurons in Parkinson's disease models. Proc Natl Acad Sci USA 104:14430–14435
27. Bandtlow C, Dechant G (2004) From cell death to neuronal regeneration, effects of the p75 neurotrophin receptor depend on interactions with partner subunits. Sci STKE 235:pe24
28. Mi S, Sandrock A, Miller RH (2008) LINGO-1 and its role in CNS repair. Int J Biochem Cell Biol. doi:10.1016/j.biocel.2008.03.018
29. Wang J, So K-F, McCoy JM, Pepinsky RB, Mi S, Relton JK (2006) LINGO-1 antagonist promotes functional recovery and axonal sprouting after spinal cord injury. Mol Cell Neurosci 33:311–320
30. Trifunovski A, Josephson A, Ringman A, Brene S, Spenger C, Olson L (2004) Neuronal activity-induced regulation of Lingo-1. Neuroreport 15:2397–2400
31. Araki T, Sasaki Y, Milbrandt J (2004) Increased nuclear NAD biosynthesis and SIRT1 activation prevent axonal degeneration. Science 305:1010–1013
32. Sajadi A, Schneider BL, Aebischer P (2004) WldS-mediated protection of dopaminergic fibers in an animal model of Parkinson disease. Curr Biol 14:326–330
33. Mi W, Beirowski B, Gillingwater TH, Adalbert R, Wagner D, Grumme D, Osaka H, Conforti L, Arnhold S, Addicks K et al. (2005) The slow Wallerian degeneration gene, *WldS*, inhibits axonal spheroid pathology in gracile axonal dystrophy mice. Brain 128:405–416

AQ1

UNCORRECTED PROOF

34. Fischer LR, Culver DG, Davis AA, Tennant P, Wang M, Coleman M, Asress S, Adalbert R, Alexander GM, Glass JD (2005) The *Wlds* gene modestly prolongs survival in the SOD1G93A fALS mouse. Neurobiol Dis 19:293–300
35. Vande Velde C, Garcia ML, Yin X, Trapp BD, Cleveland DW (2004) The neuroprotective factor WldS does not attenuate mutant SOD1-mediated motor neuron disease. Neuromolecular Med 5:193–204
36. Ravikumar B, Vacher C, Berger Z, Davies JE, Luo S, Oroz LG, Scaravilli F, Easton DF, Duden R, O'Kane CJ et al. (2004) Inhibition of mTOR induces autophagy and reduces toxicity of polyglutamine expansions in fly and mouse models of Huntington disease. Nat Genet 36: 585–595
37. Sarkar S, Perlstein EO, Imarisio S, Pineau S, Cordenier A, Maglathlin RL, Webster JA, Lewis TA, O'Kane CJ, Schreiber SL et al. (2007) Small molecules enhance autophagy and reduce toxicity in Huntington's disease models. Nat Chem Biol 3:331–338
38. Ehninger D, Han S, Shilyansky C, Zhou Y, Li W, Kwiatkowski DJ, Ramesh V, Silva AJ (2008) Reversal of learning deficits in a Tsc2 + /− mouse model of tuberous sclerosis. Nat Med. doi:10.1038/nm1788
39. Zhang B, Maiti A, Shively S, Lakhani F, McDonald-Jones G, Bruce J, Lee E B, Xie S X, Joyce S, Li C et al. (2005) Microtubule-binding drugs offset tau sequestration by stabilizing microtubules and reversing fast axonal transport deficits in a tauopathy model. Proc Natl Acad Sci USA 102:227–231

AQ2

UNCORRECTED PROOF

Chapter-4

Query No.	Page No.	Line No.	Query
AQ1	108	18	Please provide volume and page range details for the reference (28).
AQ2	108	41	Please provide volume and page range details for the reference (38).

UNCORRECTED PROOF

nature neuroscience

© 2008 Nature Publishing Group http://www.nature.com/natureneuroscience

Astrocytes as determinants of disease progression in inherited amyotrophic lateral sclerosis

Koji Yamanaka[1,2], Seung Joo Chun[1], Severine Boillee[1], Noriko Fujimori-Tonou[2], Hirofumi Yamashita[2], David H Gutmann[3], Ryosuke Takahashi[4], Hidemi Misawa[5] & Don W Cleveland[1]

Dominant mutations in superoxide dismutase cause amyotrophic lateral sclerosis (ALS), an adult-onset neurodegenerative disease that is characterized by the loss of motor neurons. Using mice carrying a deletable mutant gene, diminished mutant expression in astrocytes did not affect onset, but delayed microglial activation and sharply slowed later disease progression. These findings demonstrate that mutant astrocytes are viable targets for therapies for slowing the progression of non–cell autonomous killing of motor neurons in ALS.

ALS is an adult-onset neurodegenerative disease, characterized by a progressive and fatal loss of motor neurons. Dominant mutations in the gene for superoxide dismutase (*SOD1*) are the most frequent cause of inherited ALS. Ubiquitous expression of mutant *SOD1* in rodents leads to progressive, selective motor neuron degeneration as a result of acquired toxic properties. The exact mechanism responsible for motor neuron degeneration in ALS, however, is not known[1,2]. Mutant damage in the vulnerable motor neurons is a key determinant of disease onset[3], whereas accumulating evidence supports an active role of non-neuronal cells in motor neuron degeneration[3–7]. Evidence with selective gene excision[3] or bone-marrow grafting[5] has demonstrated that mutant SOD1-derived damage in microglia accelerates later disease progression. Despite the importance of astrocyte function, the role of mutant action in astrocytes in disease has not been tested *in vivo*.

To examine whether mutant SOD1 damage in astrocytes contributes to disease, *loxSOD1*^{G37R} mice[3], carrying a mutant *SOD1* gene that can be deleted by the action of the Cre recombinase, were mated with *GFAP-Cre* mice (**Fig. 1** and **Supplementary Fig. 1** online), which express both Cre recombinase and β-galactosidase (*LacZ*) under the control of the human GFAP promoter[8]. Mice from these matings that carry the *GFAP-Cre* transgene are denoted as Cre$^+$, whereas mice without it are referred to as Cre$^-$. To determine the cell-type specificity of Cre expression in the spinal cord, *GFAP-Cre* mice were mated to Rosa26 mice, which ubiquitously express a *LacZ* gene that encodes functional β-galactosidase only after Cre-mediated recombination. Although this *GFAP-Cre* transgene is expressed in a subset of neurons in the cerebellum and hippocampus during embryogenesis[9], measurement of β-galactosidase activity (by deposition of a blue reaction product after addition of the X-gal substrate) demonstrated that Cre expression and Cre-mediated recombination was restricted in the spinal cord to GFAP-reactive astrocytes (**Fig. 1a,b**). The efficiency of mutant gene excision in cultured astrocytes from newborn *loxSOD1*^{G37R}*/GFAP-Cre*$^+$ mice was ~76% (**Fig. 1d,e**), determined by quantitative PCR for human SOD1 transgene number (**Fig. 1d**) and immunoblotting for mutant SOD1 levels (**Fig. 1e**). We observed neither detectable Cre activity nor mutant gene excision in microglia (**Fig. 1c** and **Supplementary Fig. 2** online).

A simple, objective measure of disease onset and early disease was applied by initiation of weight loss, itself reflecting denervation-induced muscle atrophy. Reduction of SOD1^{G37R} in astrocytes did not slow disease onset nor early disease (GFAP-Cre$^+$, 341.6 ± 48.9 d; GFAP-Cre$^-$, 337.0 ± 35.8 d; **Fig. 1f,h**). However, late disease progression (from early disease to end stage) was sharply delayed, providing a mean extension of survival by 48 d (Cre$^+$, 87.4 d; Cre$^-$, 39.5 d; **Fig. 1j**). Progression from onset to early disease was more modestly slowed by 14 d (Cre$^+$, 99.3 d; Cre$^-$, 85.2 d; **Fig. 1i**). Overall survival was extended by 60 d (Cre$^+$, 436.5 ± 38.8 d; Cre$^-$, 376.5 ± 26.9 d; **Fig. 1g**). This contrasts with delayed disease onset from diminished mutant synthesis solely within motor neurons (with a *VAChT-Cre* transgene carrying the motor neuron–specific vesicular acetylcholine transporter promoter) without affecting disease progression (**Supplementary Results, Supplementary Methods** and **Supplementary Fig. 3** online), just as reported previously with an *Isl1* (*Islet1*)*-Cre* transgene that is expressed in motor neurons and some peripheral tissues[3].

Astrocytic and microglial cell activation is a well-accepted feature of SOD1 mutant–mediated ALS[1,2]. An elevated proportion of GFAP-positive astrocytes appeared before disease onset (**Fig. 2a**) in *loxSOD1*^{G37R} mice. This astrogliosis was progressive, readily apparent by onset (**Fig. 2b**) and more prominent during disease progression (**Fig. 2c**). Despite substantial mutant reduction, astrogliosis was not, however, different in comparing disease-matched *loxSOD1*^{G37R}*/GFAP-Cre*$^+$ mice (**Fig. 2d,e**) and *loxSOD1*^{G37R}*/GFAP-Cre*$^-$ mice (**Fig. 2b,c**).

Microglial activation occurred at earliest disease onset in *Cre*$^-$ mice (**Fig. 2g**) and was progressively more prominent during disease progression (**Fig. 2h**). Microglial activation was, however, substantially delayed from onset through early disease in the *GFAP-Cre*$^+$ mice when mutant SOD1 levels were reduced only in astrocytes (**Fig. 2i,j**). By exploiting the presence of β-galactosidase to mark astrocytes with diminished SOD1 mutant synthesis, examination of sections throughout lumbar spinal cords of symptomatic *loxSOD1*^{G37R}*/GFAP-Cre*$^+$ mice

[1]Ludwig Institute for Cancer Research and Department of Medicine and Neuroscience, University of California at San Diego, 9500 Gilman Drive, La Jolla, California 92093-0670, USA. [2]Yamanaka Research Unit, RIKEN Brain Science Institute, 2-1 Hirosawa, Wako, Saitama 351-0198, Japan. [3]Department of Neurology, Washington University School of Medicine, 660 South Euclid Avenue, St. Louis, Missouri 63110, USA. [4]Department of Neurology, Graduate School of Medicine, Kyoto University, 54 Shogoin Kawahara-cho, Sakyo-ku, Kyoto 606-8507, Japan. [5]Department of Pharmacology, Kyoritsu University of Pharmacy, 1-5-30 Shibakoen, Minato-ku, Tokyo 105-8512, Japan. Correspondence should be addressed to D.W.C. (dcleveland@ucsd.edu) or K.Y. (kyamanaka@brain.riken.jp).

Received 26 November 2007; accepted 7 January 2008; published online 3 February 2008; doi:10.1038/nn2047

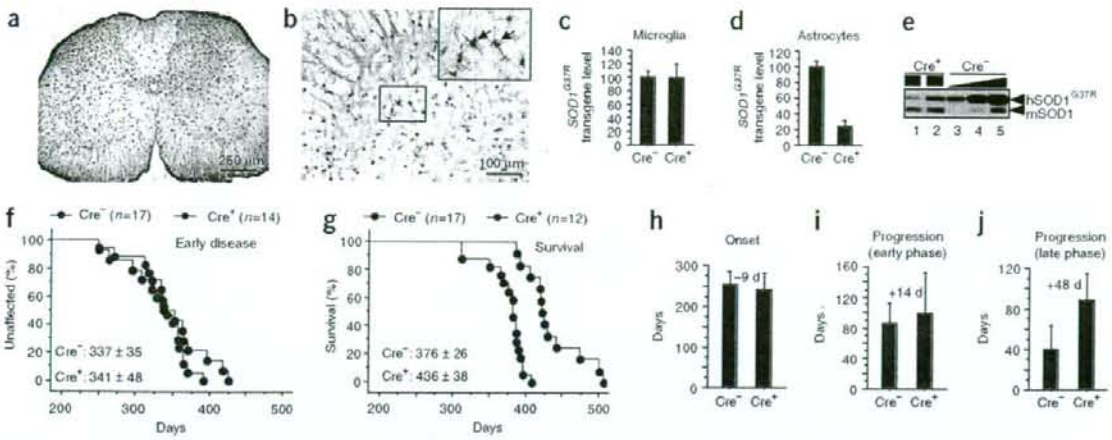

Figure 1 Selective Cre-mediated gene excision shows that mutant SOD1 action in astrocytes is a primary determinant of late disease progression. (**a**,**b**) β-galactosidase (β-gal) activity in astrocytes in whole (**a**) or in the anterior horn region (**b**) of the lumbar spinal cord section of *GFAP-Cre*/Rosa26 reporter mice visualized with X-gal and immunostaining with GFAP antibody. Inset, magnified image of the boxed area in **b**. Arrows indicate β-gal/GFAP-Cre–expressing astrocytes. (**c**,**d**) *loxSOD1*^{G37R} transgene levels ($n = 3$ for each group) in primary microglia (**c**) or astrocytes (**d**) from *loxSOD1*^{G37R}/*GFAP-Cre*$^{+}$ and *loxSOD1*^{G37R} mice using real-time PCR. (**e**) We determined SOD1^{G37R} and mouse SOD1 levels by immunoblotting extracts from isolated primary astrocytes of *loxSOD1*^{G37R}/*GFAP-Cre*$^{+}$ (lanes 1, 2) and a dilution series of a comparable extract from LoxSOD1^{G37R} astrocytes representing 25%, 50% and 100% of the protein amounts loaded in lanes 1 and 2 (lanes 3–5). (**f**,**g**) Ages at which early disease phase (to 10% weight loss, $P = 0.76$; **f**) or end-stage disease ($P < 0.0001$; **g**) were reached for *loxSOD1*^{G37R}/*GFAP-Cre*$^{+}$ mice (red) and *loxSOD1*^{G37R} littermates (blue). Mean ages ± s.d. are provided. (**h**–**j**) Mean onset ($P = 0.47$) (**h**), mean duration of early disease (from onset to 10% weight loss, $P = 0.35$; **i**) and a late disease (from 10% weight loss to end stage, $P < 0.0001$; **j**) for *loxSOD1*^{G37R}/*GFAP-Cre*$^{+}$ (red) and *loxSOD1*^{G37R} littermates (blue). At each time point, *P* value was determined by unpaired *t*-test. Error bars denote s.d.

revealed an inverse relationship (**Fig. 3a–g**) between the number of astrocytes with reduced mutant SOD1 (*Cre*$^{+}$) and activated microglia (correlation coefficient, $r = -0.868$, $P < 0.001$), despite comparable astrocytic activation. Thus, microglial activation was most prominent in areas with the highest mutant SOD1–expressing astrocyte concentration.

Elevated production of nitric oxide by upregulated inducible nitric oxide synthase (iNOS) has been reported in mutant SOD1 mice[10], although deletion of the iNOS gene has modest[11] or no[12] effect on SOD1-mediated disease. It is not known in which glial cells this nitric oxide is produced in *in vivo* models of ALS, although both microglia and astrocytes have an ability to produce it when stimulated *in vitro*[13]. Triple staining of lumbar spinal cord sections with iNOS, Mac2 and GFAP antibodies (**Fig. 3h–r**) revealed that almost all iNOS-positive cells were Mac2-positive microglia (**Fig. 3n–r** and **Supplementary Fig. 4** online), indicating that activated microglia are the primary cell type producing nitric oxide in this SOD1 mouse model. Diminishing mutant synthesis in astrocytes inhibited iNOS induction in disease-matched, symptomatic SOD1 mice (**Fig. 3h,k**), consistent with substantial inhibition of microglial activation (**Fig. 3i,l**).

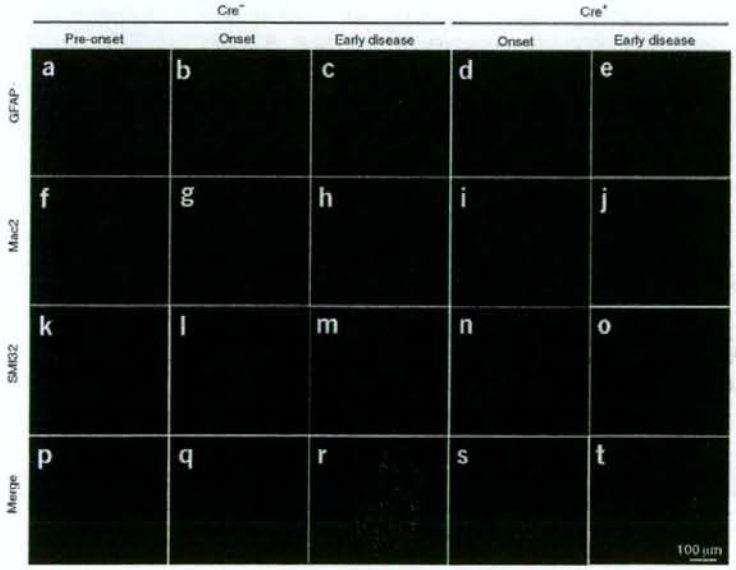

Figure 2 Selective downregulation of mutant SOD1 in astrocytes significantly inhibits microglial activation. (**a**–**t**) GFAP-positive astrocytes (**a**–**e**), Mac2-positive activated microglia (**f**–**j**) and motor neurons identified with the neurofilament antibody SMI-32 (**k**–**o**) in the lumbar spinal cord of a *loxSOD1*^{G37R} mouse before disease onset (**a**,**f**,**k**,**p**), at disease onset (**b**,**g**,**l**,**q**) or during early disease (**c**,**h**,**m**,**r**), together with *loxSOD1*^{G37R}/*GFAP-Cre*$^{+}$ mice at disease onset (**d**,**i**,**n**,**s**) or during early disease (**e**,**j**,**o**,**t**). Merged images are shown in **p**–**t**.

© 2008 Nature Publishing Group http://www.nature.com/natureneuroscience

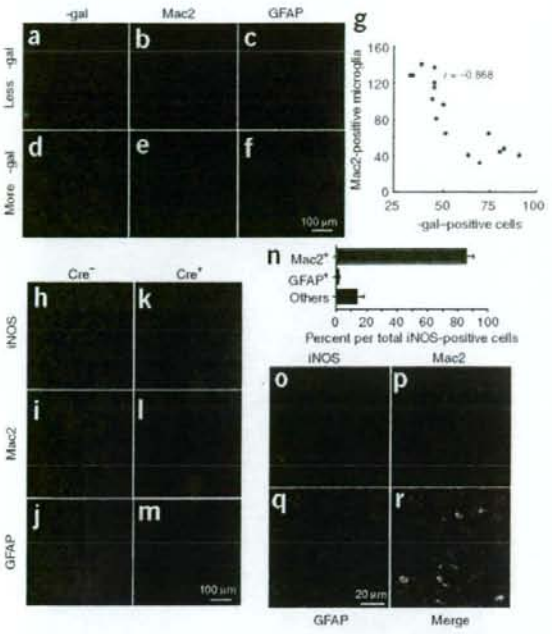

Figure 3 Mutant-expressing astrocytes enhance microglial activation and induction of iNOS. (**a–f**) Images of β-galactosidase (**a,d**), Mac2 (**b,e**) and GFAP (**c,f**) staining from a left (**a–c**) and right (**d–f**) lumbar spinal cord section from a 12-month-old *loxSOD1*^{G37R}*/GFAP-Cre*$^{+}$ mouse. *GFAP-Cre*$^{+}$ astrocytes are marked by β-galactosidase (**a,d**). (**g**) Inverted correlation between the number of Cre-positive astrocytes and Mac2-positive microglia in *loxSOD1*^{G37R}*/GFAP-Cre*$^{+}$ mice lumbar spinal cord sections (correlation coefficient, $r = -0.868$, $P < 0.001$). (**h–m**) Lumbar spinal cord sections from *loxSOD1*^{G37R} (**h–j**) and *loxSOD1*^{G37R}*/GFAP-Cre*$^{+}$ (**k–m**) mice at the early disease stage immunostained with antibodies to iNOS (**h,k**), Mac2 (**i,l**), and GFAP (**j,m**). (**n**) Quantification of iNOS-positive cells in the anterior horn from lumbar spinal cord of symptomatic *loxSOD1*^{G37R} mice. We plotted the averaged percent of iNOS^{+}/Mac2^{+} (red), iNOS^{+}/GFAP^{+} (blue) and iNOS^{+}/other cell type (black) per total iNOS^{+} cells. (**o–r**) Magnified images of anterior horn from lumbar spinal cord of symptomatic *loxSOD1*^{G37R} mice stained with iNOS (**o**), Mac2 (**p**) and GFAP (**q**). Merged image illustrates that iNOS-positive cells are Mac2-positive microglia (**r**).

A role for astrocytes in inherited ALS has been previously considered in several contexts. Mutant-expressing astrocytes produce and release one or more as yet uncharacterized components that can accelerate motor neuron death *in vitro*[6,7]. Focal loss of the astrocytic EAAT2 glutamate transporter in affected regions[14] (**Supplementary Fig. 5** online) and the failure of normal glutamate uptake of *SOD1*^{G93A} astrocytes *in vitro*[15] support glutamate-dependent excitotoxicity as a component of disease. Nevertheless, diminished mutant SOD1 synthesis in most astrocytes did not affect disease-dependent loss of EAAT2 from those astrocytes (**Supplementary Fig. 5**), indicating that a reduction in glutamate transport reflects non–cell autonomous damage to astrocytes, in part, from mutant SOD1 synthesized by other cells. Our use of selective gene excision has now demonstrated that mutant SOD1 damage in both microglia[3] and astrocytes (**Fig. 1g–j**) accelerates later disease progression without affecting the initiation of motor neuron degeneration and phenotypic disease onset. Discovery that damage in astrocytes determines the timing of microglial activation and infiltration provides further evidence that, beyond any direct effect of mutant astrocytes on motor neurons, such astrocytes amplify an inflammatory response from microglia (including enhanced production of nitric oxide and possibly of toxic cytokines), leading to further damage to the motor neurons and accelerated disease progression through a non–cell autonomous mechanism (**Supplementary Fig. 6** online). These findings validate therapies, including astrocytic stem cell–replacement approaches, that aim to slow disease progression in ALS by supplementing healthy astrocytes or modulating toxicity in astrocytes to control an inflammatory response of microglia.

Note: Supplementary information is available on the Nature Neuroscience website.

ACKNOWLEDGMENTS

This work was supported by a US National Institutes of Health grant (NS 27036) and a grant from the Packard ALS Center at Johns Hopkins (D.W.C.), as well as a Muscular Dystrophy Association developmental grant, the Uehara Memorial Foundation, the Nakabayashi Trust for ALS Research and a grant-in-aid for Scientific Research (19591021) and on Priority Area (19044048) from the Ministry of Education, Culture, Sports, Science and Technology of Japan (K.Y.). Salary support for D.W.C is provided by the Ludwig Institute for Cancer Research. S.B. is a recipient of a Fondation pour la Recherche Medical fellowship, an Institut National de la santé et de la Recherché Medicale fellowship and a Muscular Dystrophy Association developmental grant.

AUTHOR CONTRIBUTIONS

K.Y., S.J.C., S.B., N.F.-T. and H.Y. conducted the experiments. D.H.G., R.T. and H.M. provided essential experimental tools and advice. K.Y., S.B., and D.W.C. were responsible for the overall design of the project, analyses of the results and writing the manuscript.

Published online at http://www.nature.com/natureneuroscience
Reprints and permissions information is available online at http://npg.nature.com/reprintsandpermissions

1. Pasinelli, P. & Brown, R.H. *Nat. Rev. Neurosci.* **7**, 710–723 (2006).
2. Boillee, S., Vande Velde, C. & Cleveland, D.W. *Neuron* **52**, 39–59 (2006).
3. Boillee, S. *et al. Science* **312**, 1389–1392 (2006).
4. Clement, A.M. *et al. Science* **302**, 113–117 (2003).
5. Beers, D.R. *et al. Proc. Natl. Acad. Sci. USA* **103**, 16021–16026 (2006).
6. Di Giorgio, F.P., Carrasco, M.A., Siao, M.C., Maniatis, T. & Eggan, K. *Nat. Neurosci.* **10**, 608–614 (2007).
7. Nagai, M. *et al. Nat. Neurosci.* **10**, 615–622 (2007).
8. Bajenaru, M.L. *et al. Mol. Cell. Biol.* **22**, 5100–5113 (2002).
9. Fraser, M.M. *et al. Cancer Res.* **64**, 7773–7779 (2004).
10. Almer, G., Vukosavic, S., Romero, N. & Przedborski, S. *J. Neurochem.* **72**, 2415–2425 (1999).
11. Martin, L.J. *et al. J. Comp. Neurol.* **500**, 20–46 (2007).
12. Son, M., Fathallah-Shaykh, H.M. & Elliott, J.L. *Ann. Neurol.* **50**, 273 (2001).
13. Barbeito, L.H. *et al. Brain Res. Brain Res. Rev.* **47**, 263–274 (2004).
14. Howland, D.S. *et al. Proc. Natl. Acad. Sci. USA* **99**, 1604–1609 (2002).
15. Vermeiren, C. *et al. J. Neurochem.* **96**, 719–731 (2006).

© 2008 Nature Publishing Group http://www.nature.com/natureneuroscience

Available online at www.sciencedirect.com
ScienceDirect
Neuroscience Research 61 (2008) 43–48
Neuroscience Research
www.elsevier.com/locate/neures

L347P PINK1 mutant that fails to bind to Hsp90/Cdc37 chaperones is rapidly degraded in a proteasome-dependent manner

Yasuhiro Moriwaki [a,b], Yeon-Jeong Kim [b], Yukari Ido [a], Hidemi Misawa [a], Koichiro Kawashima [a], Shogo Endo [c], Ryosuke Takahashi [b,d,*]

[a] *Department of Pharmacology, Kyoritsu University of Pharmacy, 1-5-30 Shibakoen, Minato-ku, Tokyo 105-8512, Japan*
[b] *Laboratory for Motor System Neurodegeneration, RIKEN Brain Science Institute, 2-1 Hiroswa, Wako-Shi, Saitama 351-0198, Japan*
[c] *Unit for Molecular Neurobiology of Learning and Memory, Initial Research Project, Okinawa Institute of Science and Technology, Uruma, Okinawa 904-2234, Japan*
[d] *Department of Neurology, Kyoto University Graduate School of Medicine, 54 Kawahara-cho, Shogoin, Sakyo-ku, Kyoto 606-8507, Japan*

Received 26 November 2007; accepted 15 January 2008
Available online 21 January 2008

Abstract

Mutation of PTEN-induced kinase 1 (*PINK1*), which encodes a putative mitochondrial serine/threonine kinase, leads to PARK6, an autosomal recessive form of familial Parkinson's disease. Although the precise function(s) of PINK1 protein is unknown, the recessive inheritance of this form of Parkinson's disease suggests loss of PINK1 function is closely associated with its pathogenesis. Here we report that PINK1 forms a complex with the molecular chaperones Hsp90 and Cdc37/p50 within cells, which appears to enhance its stability. When cells were treated with an Hsp90 inhibitor (geldanamycin or novobiocin), levels of PINK1 were greatly diminished, reflecting its rapid degradation via ubiquitin-proteasome pathway. Similarly, the half-life of a pathogenic PINK1 mutant (L347P) that did not interact with Hsp90 or Cdc37/p50 was only 30 min, whereas that of wild-type PINK1 was 1 h. These results strongly suggest that Hsp90 and Cdc37 are binding partners of PINK1 which regulate its stability.
© 2008 Elsevier Ireland Ltd and the Japan Neuroscience Society. All rights reserved.

Keywords: Parkinson's disease; PINK1; Hsp90; Cdc37; Proteasome; Stability

1. Introduction

Parkinson's disease (PD) is the second most frequently occurring neurodegenerative disorder and is characterized by selective dopaminergic neural cell loss in the substantia nigra (Dauer and Przedborski, 2003). Most cases of PD are sporadic; in 5–10% of the PD patients, however, the cause is an inherited gene mutation. Moreover, the fact that the clinical characteristics of familial PD are similar to those of sporadic PD has lead to efforts to understand the pathogenic mechanisms induced by the related gene mutations. Several genes are now known to be causally associated with familial PD (Abou-Sleiman et al., 2006). Among them, mutations in the PTEN-induced putative kinase 1 gene (*PINK1*) have been shown to be associated with an autosomal recessive form of familial PD (Valente et al., 2004).

PINK1 was initially isolated from endometrial cancer cells overexpressing PTEN (Unoki and Nakamura, 2001), and the predicted primary sequence of PINK1 protein included an N-terminal mitochondrial-targeting signal along with a catalytic serine/threonine kinase domain. Although PINK1's mitochondrial localization and self-directed phosphorylation activity have already been characterized (Valente et al., 2004; Beilina et al., 2005; Silvestri et al., 2005; Nakajima et al., 2003), its relation to the pathogenesis of PD is poorly understood. However, evidence from several recent studies suggests that PINK1 has the ability to protect cells from stress-induced mitochondrial dysfunction and apoptosis (Valente et al., 2004; Petit et al., 2005; Deng et al., 2005; Park et al., 2006; Clark et al., 2006; Tang et al., 2006). In addition, Deng et al. (2005) recently showed that suppression of PINK1 expression reduces cell viability and significantly increases 1-methyl-4-phenylpyridinium (MPP^+)- and rotenone-induced cytotoxicity. Consistent with those findings, *PINK1*-null flies exhibit male sterility,

* Corresponding author at: Department of Neurology, Kyoto University Graduate School of Medicine, 54 Kawahara-cho, Shogoin, Sakyo-ku, Kyoto 606-8507, Japan. Tel.: +81 75 751 3770; fax: +81 75 761 9780.
E-mail address: ryosuket@kuhp.kyoto-u.ac.jp (R. Takahashi).

0168-0102/$ – see front matter © 2008 Elsevier Ireland Ltd and the Japan Neuroscience Society. All rights reserved.
doi:10.1016/j.neures.2008.01.006

apoptotic muscle degeneration, defects in mitochondrial morphology and increased sensitivity to multiple stresses, including oxidative stress (Park et al., 2006; Clark et al., 2006). These data, along with the recessive nature of *PINK1* mutations, suggest that this form of familial PD is associated with the loss of PINK1 function.

On the other hand, Tang et al. (2006) showed that DJ-1, another protein causatively associated with familial PD, normally interacts with and stabilizes PINK1, and DJ-1 mutations that attenuate this interaction reduce the stability of PINK1. These findings suggest that protein–protein interactions between PINK1 and one or more unknown proteins could play a key regulatory role in affecting the activity and stability of PINK1. In the present study, therefore, we endeavored to isolate PINK1-binding partners using a combination of immunoprecipitation and mass-spectrometric analysis with the aim of obtaining additional information on the pathogenic features of PINK1 mutations. Our findings suggest that the stability of PINK1 is strongly affected by its interaction with Hsp90, and that inhibition of the PINK1–Hsp90 interaction might contribute to the pathogenesis of PD.

2. Materials and methods

2.1. Plasmids and antibodies

The coding region of human PINK1 was cloned using standard RT-PCR techniques. PINK1 mutants were generated using a QuikChange site-directed mutagenesis kit (Stratagene) according to the manufacturer's instructions. Wild-type and all mutant PINK1 cDNAs were cloned into the mammalian expression vector pcDNA3, which also contained the FLAG tag sequence at its 3′ terminal (pcDNA3-FLAG-C). Proper construction of all the plasmids was verified by DNA sequencing. Anti-FLAG (M2), anti-Hsp90 (H-114), anti-Cdc37 (C-11) and anti-HA (Y-11) Abs were purchased from Sigma or Santa Cruz.

2.2. Cell culture and transfection

COS7 and HEK293 cells were cultured in Dulbecco's modified Eagle's medium supplemented with 10% heat-inactivated fetal bovine serum (ICN Biomedical, Inc.), 50 U/ml of penicillin and 50 U/ml of streptomycin at 37 °C under an atmosphere of 95% air/5% CO_2. Plasmids encoding PINK1 cDNAs were transfected into cells using Lipofectamine or Lipofectamine 2000 (Invitrogen) according to the manufacturer's instructions.

2.3. Purification of PINK1-binding proteins

PINK1-FLAG-transfected HEK293 cells were homogenized in lysis buffer (20 mM Hepes [pH 7.4], 150 mM NaCl, 10% glycerol and 1% Triton X-100) supplemented with Complete Protease Inhibitors (Roche Diagnostics). The soluble fraction of the lysate was immunoprecipitated with anti-FLAG M2 agarose (Sigma) and then washed five times in lysis buffer without protease inhibitors. The fractions eluted with 200 μg/ml FLAG peptide were resolved by SDS-PAGE, after which the protein bands were stained with Coomassie Brilliant Blue (CBB) and excised for in-gel digestion.

2.4. Mass-spectral analysis

In-gel digestion was carried out as described by Mineki et al. (2002). Briefly, the excised protein bands were alkylated and then incubated with 12.5 ng/μl trypsin/100 mM NH_4HCO_3 overnight at 37 °C. The resultant tryptic peptides were extracted from the gel by successive incubations with (i) 50% CH_3CN/1% trifluoroacetic acid and (ii) 20% HCOOH/25% CH_3CN/15% isopropanol/40% H_2O. The extracts from each step were pooled and dried by vacuum centrifugation. For peptide mapping, we used a LCQ-Deca XP ion trap mass spectrometer with a nanoelectrospray ionization source (Thermo Electron Corp., Waltham, MA) combined with a reverse-phase capillary column (Cadenza C18, 2 mm × 50 mm, Microme BioResources, Inc., Auburn, CA) on a Magic 2002 high performance liquid chromatography system (Microme BioResources, Inc.). The MS spectra and MS/MS spectra data were collected using Xcalibur software (Matrix Science, London, UK). The data were analyzed for candidate sequences of PINK1-interacting proteins using MASCOT software (Matrix Science) with a public domain protein database (National Center for Biotechnology Information).

2.5. Treatment with Hsp90 and protease inhibitors

Geldanamycin (GA) and novobiocin were purchased from Sigma. Epoxomycin, benzyloxycarbonyl-Leu-Leu-Leu-aldehyde (MG132), pepstatin A and leupeptin were from Peptide Institute. GA (1 mM) was prepared in DMSO and used at a final concentration of 3 μM; novobiocin was prepared in water and used at a final concentration of 1 mM; MG132 (10 mM) was prepared in DMSO and used at a final concentration of 5 μM; epoxomycin (1 mM) was prepared in DMSO and used at a final concentration of 1 μM; leupeptin (1 mM) was prepared in water and used at a final concentration of 20 μM; and pepstatin (1 mM) was prepared in DMSO and used at a final concentration of 25 μM. Cells were exposed to drugs or vehicles 24 h post-transfection.

2.6. Degradation assay

COS7 cells were transiently transfected with wild-type or L347P PINK1-FLAG. Twenty-four hours after transfection, cells were treated with 100 μg/ml cycloheximide (CHX) to prevent protein synthesis, after which they were harvested in lysis buffer at the times indicated in Section 3. Protein concentrations were determined using a Coomassie Plus Protein Assay Reagent kit (Pierce), and equal amounts of protein were subjected to SDS-PAGE. The resolved proteins were transferred to PVDF membranes (Immobilon, Millipore) and analyzed by immunoblot analysis using anti-FLAG Ab, after which the bands were visualized using an enhanced chemiluminescence detection kit (Amersham Pharmacia).

3. Results

3.1. PINK1 forms a complex with both Hsp90 and Cdc37

To isolate PINK1-binding proteins, HEK293 cells were transiently transfected with C-terminal FLAG-tagged PINK1 (PINK1-FLAG), after which proteins in the cell lysates were immunoprecipitated using anti-FLAG M2 agarose, subjected to SDS-PAGE, and stained with CBB. As a control, the same purification procedure was undertaken with non-transfected HEK293 cells. We observed several bands in samples from PINK1-FLAG transfectants that were not discernable in the control sample (Fig. 1A). We then identified the proteins in those bands using standard tryptic peptide mass-spectrometric finger printing (Fig. 1B). Consistent with earlier results, two of the proteins were identified as PINK1, itself (Beilina et al., 2005; Silvestri et al., 2005; Petit et al., 2005; Park et al., 2006), while the others were identified as Hsp90, Hsp70 and Cdc37. Hsp90 and Cdc37 were previously reported to interact with a number of other protein kinases, including one encoded by the PD-related gene *LRRK2* (Gloeckner et al., 2006). We then confirmed the mass-spectral identification of PINK1-associated proteins by immunoblotting samples of the purified protein

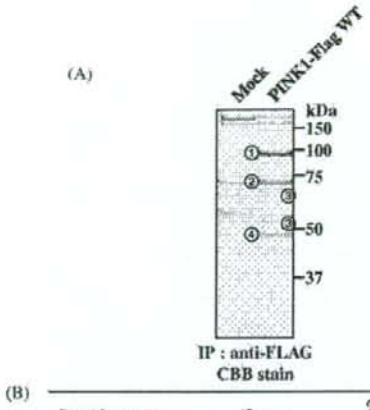

(B)

	Protein name	Score	% sequence converge
①	Hsp90	1623	56 %
②	Hsp70	720	34 %
③	PINK1	917	40 %
④	Cdc37	302	20 %

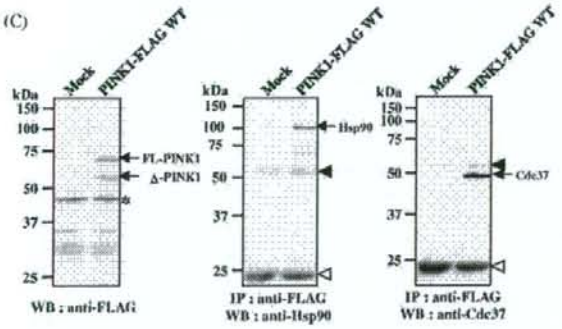

Fig. 1. PINK1 forms a complex with both Hsp90 and Cdc37. (A) HEK293 cells were transfected for 24 h with either a vector expressing PINK1-FLAG or with an empty vector (Mock). The transfectants were then lysed and immunoprecipitated with anti-FLAG Ab, the immunocomplexes were separated by SDS-PAGE, and the gel was stained with CBB to visualize proteins associated with PINK1. (B) CBB stained bands, labeled as indicated in (A), were excised from the gel and, following in-gel digestion with trypsin, their identities were determined by tryptic peptide mass-spectral fingerprinting. Scores and percentages of sequence converge for each protein identified are indicated. (C) The samples purified in (A) were immunoblotted with the indicated Abs; the asterisk indicates a non-specific band detected by anti-FALG Ab. Full length (FL) and processed PINK1 (Δ-PINK1) were detected. Closed and open arrowheads indicate IgG heavy and light chains, respectively.

with Abs against Hsp90, Cdc37 or FLAG (Fig. 1C). Taken together, these findings indicate that Hsp90 and Cdc37 specifically associate with PINK1.

3.2. Hsp90 regulates PINK1 stability

Hsp90 is a ubiquitous molecule that plays a key role in the stabilization and conformational regulation of various signaling effectors, including steroid hormone receptors and protein kinases (Young et al., 2001). To determine whether Hsp90 also regulates PINK1 stability, we next incubated COS7 cells transiently transfected with wild-type PINK1-FLAG with 1–10 μM GA, an inhibitor of Hsp90. We found that cells treated with 1 or 3 μM GA showed reduced levels of PINK1 (Fig. 2, top panel), whereas levels of Hsp90 and Cdc37 were unaffected (Fig. 2, middle and bottom panels). In addition, GA completely blocked the interaction between PINK1 and Hsp90/Cdc37. Examination of the time course of the response to GA revealed that levels of full-length PINK1 gradually declined by 90% over the course of 4 h after the addition of GA to COS7 cells (Fig. 3A). These findings were then confirmed using novobiocin, another known Hsp90 inhibitor that is structurally unrelated to GA and binds to the ATP-binding domain located in the C-terminal part of Hsp90 (Marcu et al., 2000). As shown in Fig. 3A, novobiocin treatment also significantly reduced levels of PINK1 in COS7 cells, and similar results were obtained with HEK293 cells (data not shown). The changes of PINK1 level induced by Hsp90 inhibitors are likely to be ascribable to its protein stability and degradation. First, PINK1 mRNA level was not affected by GA treatment as assessed by RT-PCR analysis (data not shown). Moreover, GA-induced PINK1 downregulation was suppressed by protease inhibitors (Fig. 3B).

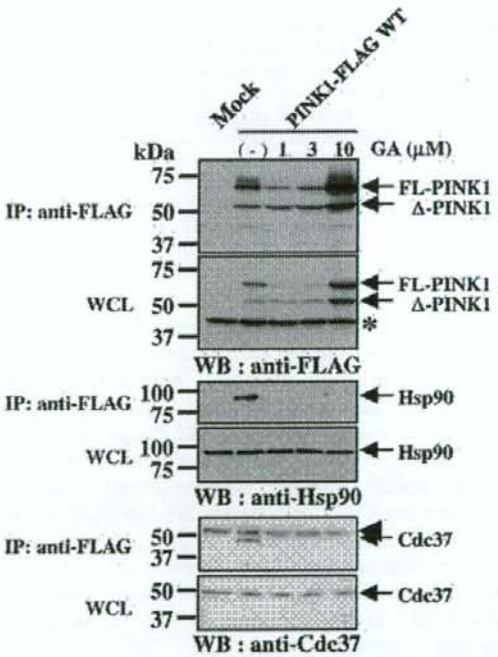

Fig. 2. GA treatment diminishes the interaction of PINK1 with both Hsp90 and Cdc37. COS7 cells were transfected for 24 h with either PINK1-FLAG or Mock expression vector and then treated with indicated concentration of GA. After incubating an additional 4 h, the cells were lysed and immunoprecipitated as described in Section 2. Immunocomplexes and whole-cell lysates (WCLs) were subjected to electrophoresis on polyacrylamide gel and immunoblotted with the indicated Abs; an asterisk indicates a non-specific band detected by anti-FALG Ab, which served as an internal control. The arrowhead indicates IgG heavy chain.

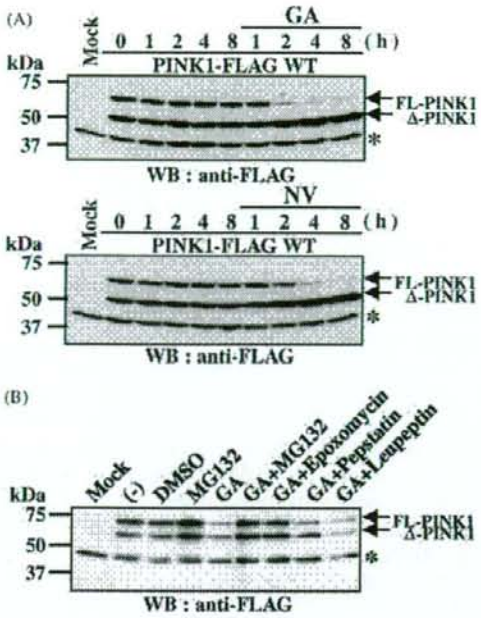

Fig. 3. PINK1 degradation is enhanced by Hsp90 inhibitors but inhibited by proteasome inhibitors. (A) COS7 cells were transiently transfected with PINK1-FLAG, after which the transfectants were incubated for the indicated times in the presence of 3 μM GA, 1 mM novobiocin (NV) or their vehicles (DMSO and water, respectively). After the indicated times or before the addition of drug (T0), the cells were lysed and their lysates were subjected to SDS-PAGE and immunoblotted with anti-FLAG M2 Ab. (B) COS7 cells transiently transfected with PINK1-FLAG were incubated for 4 h in the presence of GA or vehicle (DMSO). The proteasome inhibitors (epoxomycin or MG132) or lysosomal protease inhibitors (pepstatin or leupeptin) were simultaneously added in the presence or absence of GA. (−) indicates no drug treatment; the asterisk indicates a non-specific band detected by anti-FALG Ab, which served as an internal control.

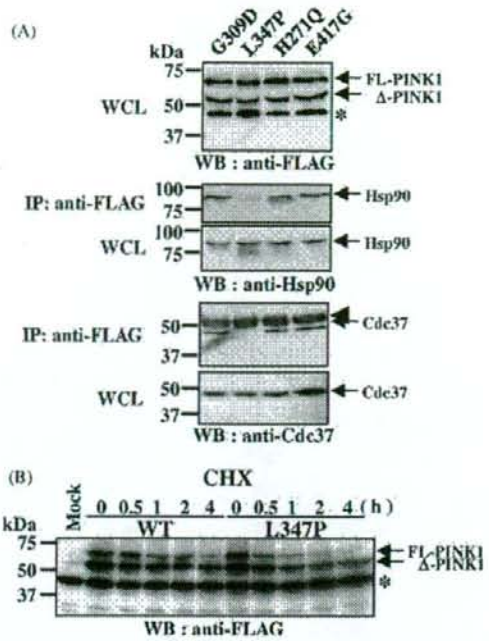

Fig. 4. Familial PD-associated L347P mutation impairs the interaction between PINK1 and Hsp90/Cdc37. (A) Wild-type PINK1 and PD-associated PINK1 mutants expressed in COS7 cells were immunoprecipitated with anti-FLAG Ab and immunoblotted with anti-Hsp90, anti-Cdc37 or anti-FLAG Ab. (B) COS7 cells were transfected for 24 h with either wild-type PINK1-FLAG or L347P mutant PINK1-FLAG, after which they were incubated for the indicated times in the presence of 100 μg/ml cycloheximide (CHX). After the indicated times or before the addition of CHX, cells were resuspended in lysis buffer, and the proteins were analyzed by immunoblotting using anti-FLAG M2 Ab. Similar results were obtained in two independent experiments. The asterisk indicates a non-specific band detected by anti-FALG Ab, which served as an internal control. The arrowhead indicates IgG heavy chain.

Several studies have shown that GA-induced degradation of Hsp90 target proteins is preceded by their ubiquitination and subsequent targeting by proteasome (Miyata et al., 2001; Nony et al., 2003; Boudeau et al., 2003; An et al., 2000). To determine whether GA-mediated decay of PINK1 is also dependent on proteasomal degradation, we blocked proteasome function using two specific inhibitors, epoxomycin and MG132. We found that when COS7 cells expressing PINK1-FLAG were incubated with GA plus either epoxomycin or MG132, but not with other protease inhibitors, degradation of full-length PINK1 was prevented (Fig. 3B). Apparently, upon dissociation of the PINK1–Hsp90 complex, PINK1 is degraded by proteasome.

3.3. Familial PD-associated L347P mutation impairs the interaction between PINK1 and Hsp90/Cdc37

Beilina et al. (2005) recently reported the L347P PINK1 mutant is much more rapidly degraded within cells than wild-type PINK1. To clarify the molecular mechanism underlying the enhanced degradation of the PINK1 mutant, we tested whether PINK1 missense mutants found in familial PD patients (Valente et al., 2004; Hatano et al., 2004) show diminished binding to Hsp90 and/or Cdc37/p50. Immunoprecipitation of PINK1 mutants using anti-FLAG Ab followed by immunoblotting with anti-Hsp90 or Cdc37/p50 Ab revealed that the L347P substitution mutant did not bind to either Hsp90 or Cdc37/p50, whereas the other PD-linked mutations we tested here did not significantly affect the interaction of PINK1 with Hsp90/Cdc37 (Fig. 4A). To confirm the effect of the L347P mutation on protein stability, we also carried out a protein degradation assay and found that the half-life of full-length wild-type PINK1 was 1 h, whereas the half-life of the full-length L347P PINK1 mutant was only 30 min (Fig. 4B). Thus the inability to bind to Hsp90 appears to substantially reduce the stability of the L347P PINK1 mutant.

4. Discussion

Our findings indicate that the molecular chaperone complex Hsp90/Cdc37 bind to PINK1 and thus regulate its stability. Hsp90 is an abundant cytoplasmic protein that functions as a

chaperone and plays an essential role in numerous cellular processes. With fewer target proteins than Hsp60 or Hsp70, Hsp90 appears to primarily bind protein kinases and hormone receptors (Young et al., 2001). To specifically interact with its client proteins, Hsp90 also requires the presence of co-chaperones. One of these, Cdc37/p50, appears to specifically target Hsp90 to a variety of protein kinases, including the mitogen-activated protein kinase (MAPK) family member MAPK-overlapping kinase (MOK) (Miyata et al., 2001), LBK1 (Nony et al., 2003; Boudeau et al., 2003), IKK (Chen et al., 2002) and LRRK2 (Gloeckner et al., 2006). One of the Hsp90/Cdc37 binding proteins IKK was reported to independently bind to both Cdc37 and Hsp90. However, treatment with Hsp90 inhibitors such as GA abolishes the binding ability of IKK to bind both Hsp90 and Cdc37, leading to disruption of its activity. These findings, along with several lines of evidence by the other researchers, suggest that Hsp90 functions in concert with Cdc37 and their interaction is important in their stabilization, activation and/or translocation. Although there is a possibility that Hsp90 and Cdc37 independently bind to PINK1, treatment with Hsp90 inhibitors markedly reduced levels of PINK1 indicate Hsp90/Cdc37 complex are key regulator for PINK1 stability.

Hsp90/Cdc37 interacts with the catalytic domains of several kinases, thereby affecting their enzymatic activity. For example, the interaction of the IKK complex with Hsp90/Cdc37 is required for its activation by tumor necrosis factor (Chen et al., 2002), and the interaction of CDK4 with Hsp90/Cdc37 is required for its proper assembly with cyclin D (Dai et al., 1996). By contrast, the kinase activity of the LKB1 is unaffected by its binding to Hsp90/Cdc37 (Nony et al., 2003). Some recent studies have shown that recombinant PINK1 expressed in *Escherichia coli* has kinase activity (Silvestri et al., 2005; Hatano et al., 2004), but it is not clear whether PINK1 expressed in mammalian cells has similar activity. In our hands, PINK1 exhibited no self-directed phosphorylation activity (data not shown). Further investigation will be required to clarify this issue.

Another function of Hsp90 is stabilization of its target proteins through the prevention of their degradation by the proteasome system. A number of oncogenes, including v-Src (An et al., 2000) and MOK (Miyata et al., 2001), are rapidly degraded in cells following treatment with GA. Consistent with the idea that Hsp90 is a key regulator of PINK1 stability, treatment with Hsp90 inhibitors markedly reduced PINK1 levels within cells (Figs. 2 and 3), while two proteasome inhibitors, epoxomycin and MG132, each prevented Hsp90-inhibitor-induced PINK1 degradation (Fig. 3).

In the present study, we found high concentration of GA treatment conversely augmented PINK1 protein level. Hsp90 was known to form complex with heat shock transcription factor Hsf1, and when this interaction was impaired by adding Hsp90 inhibitor, Hsf1 can form active trimers which enhance the transcription of a subset of genes. According to this idea, other factor(s) induced by Hsf1 may also influence on PINK1 stability.

Beilina et al. (2005) showed that when expressed in either *E. coli* or mammalian cells, steady-state level of the L347P PINK1 mutant is low. They suggested this was the result of enhanced degradation caused by disruption of α-helix similar to that observed in the L166P DJ-1 mutant (Miller et al., 2003). However, we did not observe low steady-state level of L347P PINK1 mutant protein expressed in *E. coli* (data not shown). Instead, the present results suggest that the diminished stability of the L347P PINK1 mutant reflects its inability to interact with Hsp90/Cdc37.

PINK1 reportedly reduces basal neuronal pro-apoptotic activity and protects neurons from staurosporine-induced apoptosis (Silvestri et al., 2005). In addition, Deng et al. (2005) showed that treating cells with PINK1-specific siRNA reduced their viability and significantly increased the cytotoxicity of MPP^+ and rotenone. We found that the L347P mutation diminishes both the interaction of PINK1 with Hsp90 and its stability. These results indicate that L347P mutant PINK1 loses its cell protective function due to destabilization, resulting in the development of PD. Moreover, the present results suggest possible contribution of chaperon system, especially Hsp90, to the pathogenesis of PARK6.

During the preparation of this manuscript, Weihofen et al. (2007) reported that PINK1 interact with Hsp90/Cdc37 complex. They showed GA treatment that affects Hsp90 and client protein interaction preferentially reduced the level of endogenous full-length PINK1. Our findings are consistent with their observations (Figs. 2 and 3). In the present study, we, for the first time, showed that L347P mutant PINK1 displayed diminished interaction with Hsp90/Cdc37, resulting in its instability. Again, these results indicate that L347P mutant PINK1 loses its cell protective function due to destabilization, leading to the development of PD.

Acknowledgements

We thank Dr. Yasuyuki Suzuki for his critical advice and helpful discussions. This study was supported in part by research grants from RIKEN BSI, and a grant-in-aid from the Ministry of Education, Culture, Sports, and Technology of Japan.

References

Abou-Sleiman, P.M., Muqit, M.M., Wood, N.W., 2006. Expanding insights of mitochondrial dysfunction in Parkinson's disease. Nat. Rev. Neurosci. 7, 207–219 review.

An, W.G., Schulte, T.W., Neckers, L.M., 2000. The heat shock protein 90 antagonist geldanamycin alters chaperone association with p210bcr-abl and v-src proteins before their degradation by the proteasome. Cell Growth Differ. 11, 355–360.

Beilina, A., Van Der Brug, M., Ahmad, R., Kesavapany, S., Miller, D.W., Petsko, G.A., Cookson, M.R., 2005. Mutations in PTEN-induced putative kinase 1 associated with recessive parkinsonism have differential effects on protein stability. Proc. Natl. Acad. Sci. U.S.A. 102, 5703–5708.

Boudeau, J., Deak, M., Lawlor, M.A., Morrice, N.A., Alessi, D.R., 2003. Heat-shock protein 90 and Cdc37 interact with LKB1 and regulate its stability. Biochem. J. 370, 849–857.

Chen, G., Cao, P., Goeddel, D.V., 2002. TNF-induced recruitment and activation of the IKK complex require Cdc37 and Hsp90. Mol. Cell 9, 401–410.

Clark, I.E., Dodson, M.W., Jiang, C., Cao, J.H., Huh, J.R., Seol, J.H., Yoo, S.J., Hay, B.A., Guo, M., 2006. Drosophila pink1 is required for mitochondrial function and interacts genetically with parkin. Nature 441, 1162–1166.

Dai, K., Kobayashi, R., Beach, D., 1996. Physical interaction of mammalian CDC37 with CDK4. J. Biol. Chem. 271, 22030–22034.

Dauer, W., Przedborski, S., 2003. Parkinson's disease: mechanisms and models. Neuron 39, 889–909 review.

Deng, H., Jankovic, J., Guo, Y., Xie, W., Le, W., 2005. Small interfering RNA targeting the PINK1 induces apoptosis in dopaminergic cells SH-SY5Y. Biochem. Biophys. Res. Commun. 337, 1133–1138.

Gloeckner, C.J., Kinkl, N., Schumacher, A., Braun, R.J., O'Neill, E., Meitinger, T., Kolch, W., Prokisch, H., Ueffing, M., 2006. The Parkinson disease causing LRRK2 mutation I2020T is associated with increased kinase activity. Hum. Mol. Genet. 15, 223–232.

Hatano, Y., Li, Y., Sato, K., Asakawa, S., Yamamura, Y., Tomiyama, H., Yoshino, H., Asahina, M., Kobayashi, S., Hassin-Baer, S., Lu, C.S., Ng, A.R., Rosales, R.L., Shimizu, N., Toda, T., Mizuno, Y., Hattori, N., 2004. Novel PINK1 mutations in early-onset parkinsonism. Ann. Neurol. 56, 424–427.

Marcu, M.G., Chadli, A., Bouhouche, I., Catelli, M., Neckers, L.M., 2000. The heat shock protein 90 antagonist novobiocin interacts with a previously unrecognized ATP-binding domain in the carboxyl terminus of the chaperone. J. Biol. Chem. 275, 37181–37186.

Miller, D.W., Ahmad, R., Hague, S., Baptista, M.J., Canet-Aviles, R., McLendon, C., Carter, D.M., Zhu, P.P., Stadler, J., Chandran, J., Klinefelter, G.R., Blackstone, C., Cookson, M.R., 2003. L166P mutant DJ-1, causative for recessive Parkinson's disease, is degraded through the ubiquitin-proteasome system. J. Biol. Chem. 278, 36588–36595.

Mineki, R., Taka, H., Fujimura, T., Kikkawa, M., Shindo, N., Murayama, K., 2002. In situ alkylation with acrylamide for identification of cysteinyl residues in proteins during one- and two-dimensional sodium dodecyl sulphate-polyacrylamide gel electrophoresis. Proteomics 2, 1672–1681.

Miyata, Y., Ikawa, Y., Shibuya, M., Nishida, E., 2001. Specific association of a set of molecular chaperones including HSP90 and Cdc37 with MOK, a member of the mitogen-activated protein kinase superfamily. J. Biol. Chem. 276, 21841–21848.

Nakajima, A., Kataoka, K., Hong, M., Sakaguchi, M., Huh, N.H., 2003. BRPK, a novel protein kinase showing increased expression in mouse cancer cell lines with higher metastatic potential. Cancer Lett. 201, 195–201.

Nony, P., Gaude, H., Rossel, M., Fournier, L., Rouault, J.P., Billaud, M., 2003. Stability of the Peutz-Jeghers syndrome kinase LKB1 requires its binding to the molecular chaperones Hsp90/Cdc37. Oncogene 22, 9165–9175.

Park, J., Lee, S.B., Lee, S., Kim, Y., Song, S., Kim, S., Bae, E., Kim, J., Shong, M., Kim, J.M., Chung, J., 2006. Mitochondrial dysfunction in Drosophila PINK1 mutants is complemented by parkin. Nature 441, 1157–1161.

Petit, A., Kawarai, T., Paitel, E., Sanjo, N., Maj, M., Scheid, M., Chen, F., Gu, Y., Hasegawa, H., Salehi-Rad, S., Wang, L., Rogaeva, E., Fraser, P., Robinson, B., St. George-Hyslop, P., Tandon, A., 2005. Wild-type PINK1 prevents basal and induced neuronal apoptosis, a protective effect abrogated by Parkinson disease-related mutations. J. Biol. Chem. 280, 34025–34032.

Silvestri, L., Caputo, V., Bellacchio, E., Atorino, L., Dallapiccola, B., Valente, E.M., Casari, G., 2005. Mitochondrial import and enzymatic activity of PINK1 mutants associated to recessive parkinsonism. Hum. Mol. Genet. 14, 3477–3492.

Unoki, M., Nakamura, Y., 2001. Growth-suppressive effects of BPOZ and EGR2, two genes involved in the PTEN signaling pathway. Oncogene 20, 4457–4465.

Tang, B., Xiong, H., Sun, P., Zhang, Y., Wang, D., Hu, Z., Zhu, Z., Ma, H., Pan, Q., Xia, J.H., Xia, K., Zhang, Z., 2006. Association of PINK1 and DJ-1 confers digenic inheritance of early-onset Parkinson's disease. Hum. Mol. Genet. 15, 1816–1825.

Valente, E.M., Abou-Sleiman, P.M., Caputo, V., Muqit, M.M., Harvey, K., Gispert, S., Ali, Z., Del Turco, D., Bentivoglio, A.R., Healy, D.G., Albanese, A., Nussbaum, R., Gonzalez-Maldonado, R., Deller, T., Salvi, S., Cortelli, P., Gilks, W.P., Latchman, D.S., Harvey, R.J., Dallapiccola, B., Auburger, G., Wood, N.W., 2004. Hereditary early-onset Parkinson's disease caused by mutations in PINK1. Science 304, 1158–1160.

Weihofen, A., Ostaszewski, B., Minami, Y., Selkoe, D.J., 2007. Pink1 Parkinson mutations, the Cdc37/Hsp90 chaperones and Parkin all influence the maturation or subcellular distribution of Pink1. Hum. Mol. Genet. (Epub ahead of print).

Young, J.C., Moarefi, I., Hartl, F.U., 2001. Hsp90: a specialized but essential protein-folding tool. J. Cell Biol. 154, 267–273.

		G	T	C	1	1	6	9	Operator: Zheng Yuexia	Dispatch: 19.02.08	PE: Jiaying Wang
	Journal Name				Manuscript No.				Proofreader: Tang FoYu	No. of Pages: 13	Copy-editor: Elango A.

Rines/RNF180, a novel RING finger gene-encoded product, is a membrane-bound ubiquitin ligase

Miyuki Ogawa[1,2], Kiyomi Mizugishi[3], Akira Ishiguro[1], Yoshio Koyabu[3], Yuzuru Imai[4], Ryosuke Takahashi[4], Katsuhiko Mikoshiba[2,3] and Jun Aruga[1,*]

[1]*Laboratory for Comparative Neurogenesis, RIKEN Brain Science Institute, Wako-shi, Saitama 351-0198, Japan*
[2]*Division of Molecular Neurobiology, Department of Basic Medical Science, Institute of Medical Science, University of Tokyo, Minato-ku, Tokyo 108-8639, Japan*
[3]*Laboratory for Developmental Neurobiology, RIKEN Brain Science Institute, Wako-shi, Saitama 351-0198, Japan*
[4]*Laboratory for Motor System Neurodegeneration, RIKEN Brain Science Institute, Wako-shi, Saitama 351-0198, Japan*

We identified and characterized a novel RING finger gene, *Rines/RNF180*, which is well conserved among vertebrates. Putative *Rines* gene product (Rines) contains a RING finger domain, a basic coiled-coil domain, a novel conserved domain (DSPRC) and a C-terminal hydrophobic region that is predicted to be a transmembrane domain. N-terminally epitope tagged-Rines (Nt-Rines) was detected in the endoplasmic reticulum membrane/nuclear envelope in cultured mammalian cells. Nt-Rines was not extracted by high salt or alkaline buffers and was degraded in intact endoplasmic reticulum treated with proteinase K, indicating that Nt-Rines is an integral membrane protein with most of its N-terminal regions in the cytoplasm. *Rines* was expressed in brain, kidney, testis, and uterus of adult mice, and in developing lens and brain, particularly in the ventricular layer of the cerebral cortex at embryonic stages. In cultured cells, Nt-Rines can bind another protein and promoted its degradation. The degradation was inhibited by proteasomal inhibitors. In addition, Nt-Rines itself was heavily ubiquitinated and degraded by proteasome. The involvement of Rines in the ubiquitin–proteasome pathway was further supported by its binding to the UbcH6 ubiquitin-conjugating enzyme and by its trans-ubiquitination enhancing activities. These results suggest that Rines is a membrane-bound E3 ubiquitin ligase.

Introduction

Protein degradation by the proteasome pathway plays a vital role in controlling the level of proteins involved in diverse cellular processes, including differentiation, proliferation and apoptosis (Hershko & Ciechanover 1998; Pickart 2001). In the ubiquitin–proteasome pathway, substrates are marked by covalent linkage to ubiquitin for degradation. The ubiquitinated proteins are then recognized and degraded by the 26S proteasome. Ubiquitination involves highly specific enzyme cascades such as E1 ubiquitin-activating enzyme, E2 ubiquitin-conjugating enzyme and E3 ubiquitin-protein ligase (Hershko & Ciechanover 1998; Pickart 2001). Among them, E3 ubiquitin ligase plays a key role in determining the specificity and timing of the ubiquitination of substrates and subsequent protein degradation. Many E3 ubiquitin ligases contain a RING finger domain as a binding domain for E2 enzymes (Joazeiro & Weissman 2000; Pickart 2001).

A novel RING finger motif-containing gene, *Rines*, was found in a screening for binding partner of Zic2, which belongs to the Zic family nuclear zinc finger proteins (Aruga *et al.* 1996; Nagai *et al.* 2000; Mizugishi *et al.* 2004). Because a putative *Rines* gene product (Rines) does not show any close similarities to previously known proteins, its basic molecular properties were investigated using Zic2 as a tool protein. We characterized the structure, subcellular localization, topology and molecular functions of Rines, together with the expression profiles of *Rines* in developing and adult mice. We found that *Rines* was expressed in developing and mature brain and in other organs. Rines possessed a RING finger domain that is necessary for ubiquitin ligase activity and a novel domain, and was an integral membrane protein located

Communicated by: Hiroshi Hamada
**Correspondence*: E-mail: jaruga@brain.riken.jp

DOI: 10.1111/j.1365-2443.2008.01169.x
© 2008 The Authors
Journal compilation © 2008 by the Molecular Biology Society of Japan/Blackwell Publishing Ltd.

mainly on the cytoplasmic side of the endoplasmic reticulum. Molecular function analyses revealed proteasomal degradation-enhancing, degradation target-binding and E2 enzyme-binding activities. Our results indicated Rines to be a novel proteasomal degradation mediator.

Results

Structural features of the Rines

In a yeast-two hybrid screening of an E10.5 mouse embryonic cDNA library using an entire N-terminal half of the mouse Zic2 protein (1–255) as a bait (Mizugishi *et al.* 2004), we isolated a clone that encodes part of a novel RING finger motif, the gene of which we named *Rines* (An abbreviation of *RING finger protein in neural stem cells*).

Nucleotide sequencing of the *Rines* cDNA revealed that the putative open reading frame (ORF) contains 1773 nucleotides (591 amino acids, accession: AAH46775, also named as *RNF180* in a cDNA collection project (Strausberg *et al.* 2002)). The predicted *Rines* gene product (Rines) is a 65 kDa protein containing a RING finger domain (Fig. 1A–C). The RING finger domain is a cysteine/histidine rich (C3HC4), Zn^{2+} binding domain that has been found in a number of eukaryotic proteins and considered to be chemical catalysts and molecular scaffolds that bring other proteins together (Borden 2000). Emerging evidence indicates that RING finger motif may have ubiquitin ligase activity and function in protein ubiquitination (Joazeiro & Weissman 2000; Pickart 2001). In its C-terminal end, there is a hydrophobic region, which is predicted to be a transmembrane segment by computer programs (SOSUI, Hirokawa *et al.* 1998, PHDHTM, Rost *et al.* 1996).

A homology search against BLAST/NCBI database revealed the presence of the mouse Rines homologues in human, chick, and zebrafish (Fig. 1B). The RING finger domain was strongly conserved among the Rines homologues. In addition, there were three conserved domains in an N-terminal region, an N-terminal flanking of the RING finger domain and a C-terminal portion. A homology search revealed that the N-terminally located conserved domains had a significant homology to proteins including dual specificity protein phosphatases, rat GKAP (Munoz-Alonso *et al.* 2000) and yeast Yvh1 (Giaever *et al.* 2002) (Fig. 1D). This conserved domain (named here as DSPRC, dual specificity phosphatase–Rines-conserved) is consisted of about 50 amino acids residues where four cysteine residues are absolutely conserved, and is also detected in insect and plant proteins. However, functional significance of DSPRC is not clear at this point. The second conserved region contained a cluster of basic residues. In addition, a computer program (ISREC-Coil server, <http://www.isrec.isb-sib.ch/cgi-bin/COILS-from-paser>) predicted the presence of a coiled-coil structure, which is known to mediate protein-to-protein interaction. The coiled-coil domain was also predicted in all the vertebrate Rines homologues. In the current protein database, we did not find any other proteins with a domain organization similar to that of Rines (Fig. 1A), suggesting that Rines is a unique protein.

Rines is a membrane-anchored protein

We first characterized Rines in terms of its subcellular localization. When N-terminally Flag epitope-tagged Rines (Flag-Rines) was produced in cells, it was detected as reticular staining in the cytoplasmic region (Fig. 2A). The staining greatly overlapped that of Calnexin, an endoplasmic reticulum (ER)-anchored integral membrane protein, suggesting ER membrane/nuclear envelope localization of Rines. Similarly to Calnexin, Flag-Rines was extracted from membrane fractions only in buffers containing detergents, but not in the presence of urea, salt alone or an alkaline buffer (Fig. 2B). In contrast, Calreticulin, a peripheral membrane protein of the ER, was extracted from the membrane fractions in an alkaline buffer (Fig. 2B). Peripheral membrane proteins can be separated from integral membrane proteins by extraction with 0.1 M Na_2CO_3 (Fujiki *et al.* 1982). These results indicate that Flag-Rines is an integral membrane protein, in agreement with the presence of the predicted transmembrane region. When the crude membrane fraction was treated with proteinase K in the absence of detergent, N-terminally Myc-tagged Rines was digested similarly to the ER membrane protein TRAPα, whereas BiP, an intraluminal ER protein, was mostly not (Fig. 2C). This result indicates that most of the N-terminus of Myc-Rines is located in the cytoplasm.

Expression pattern of *Rines*

The expression profile of *Rines* in mice was first examined by Northern blot analysis (Fig. 3A,B). In adult mice, the *Rines* mRNA was most strongly detected in brain, moderately in kidney, testis and uterus and weakly in lung and thymus (Fig. 3A). In the course of development, significant expression was detected from E10.5, the mRNA level was gradually increased, peaked around E13.5 and then gradually decreased (Fig. 3B). These results suggest that *Rines*, in principle, could play a role in the later gestational development.

To determine the spatial expression pattern of *Rines*, we performed a series of *in situ* hybridization histochemical

© 2008 The Authors
Journal compilation © 2008 by the Molecular Biology Society of Japan/Blackwell Publishing Ltd.

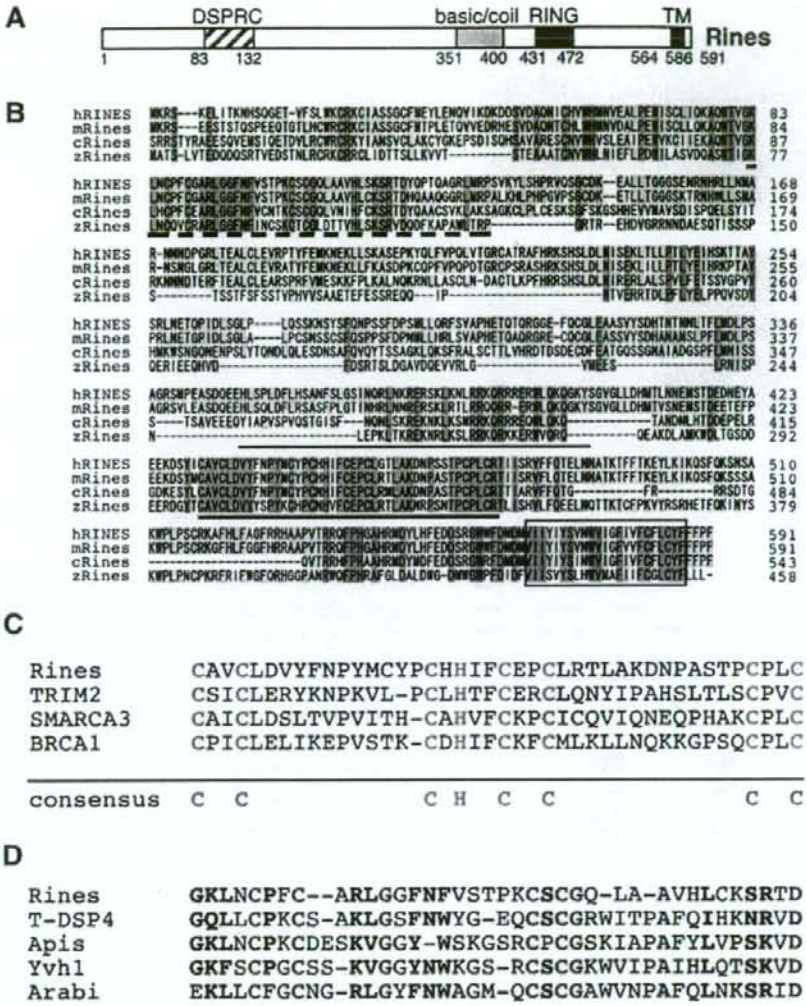

Figure 1 Structure of the Rines. (A) The domain structure of mouse Rines. *DSPRC*, dual specificity protein phosphatase Rines conserved domain; *basic/coil*, basic coiled-coil domain; *RING*, RING finger domain; *TM*, transmembrane domain. (B) Alignment of the amino acid sequences of the human (accession: CAD89939), mouse (accession: AAH46775), chick (accession: XP_429137), and zebrafish (accession: NP_956723) Rines. *Dark green boxes* indicate the conserved amino acids across the four species, and *light green boxes* indicate the conserved amino acids among the three species. *Open box*, transmembrane domain; *thick underline*, RING finger domain; *thin underline*, basic coiled-coil domain; *broken underline*, DSPRC domain. (C) Comparison of the RING finger domain amino acid sequences between mouse *Rines*, human *TRIM2*, human *SMARCA3* and human *BRCA1*. (D) Comparison of DSPRC domain sequences derived from rat glucokinase-associated phosphatase (*T-DSP4*, NP_071584), *Saccharomyces cerevisiae* Yvh1p (*Yvh1*, NP_012292), *Arabidopsis thaliana* dual specificity protein phosphatase-related protein (*Arabi*, NP_5678561), and an *Apis mellifera* protein (*Apis*, XP_396430).

© 2008 The Authors
Journal compilation © 2008 by the Molecular Biology Society of Japan/Blackwell Publishing Ltd.

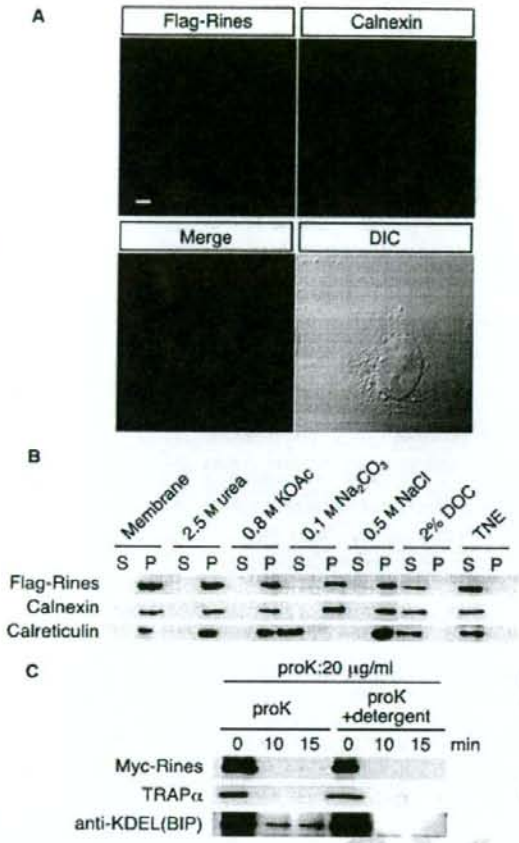

Figure 2 Localization of Rines in cultured cells. (A) Immunofluorescence staining of COS7 cells expressing Flag-Rines. Anti-Calnexin antibody was used to stain a typical ER membrane protein. Blue indicates DAPI-stained nucleus. Scale bar, 5 μm. (B) Membrane preparations of 293T cells expressing Flag-Rines were extracted with buffer containing the materials indicated. *TNE* buffer (150 mM Tris–HCl, pH 7.5; 500 mM NaCl; 1 mM EDTA; 1% Triton X-100; 0.1% SDS). *P*, pellet; *S*, supernatant. Each fraction was subjected to immunoblotting with antibodies against Flag-epitope, Calnexin (an integral membrane protein in ER) and Calreticulin (a peripheral membrane protein in ER). (C) N-termini of the Rines are oriented mostly toward the cytoplasm. Protease protection assay of N-terminally Myc-tagged Rines, an ER luminal control *BiP* (Grp78) and an integral ER membrane protein *TRAPα*. The crude membrane fraction prepared from 293T cells expressing Myc-Rines was treated with only proteinase K or with proteinase K with detergent buffer (TNE) for the time indicated. Samples were subjected to immunoblotting using the antibodies indicated.

staining using brains from E13.5 to E17.5 mouse embryos. Throughout these stages, a high level of *Rines* expression was detected in ventricular zone of the lateral ventricle while a low level of expression could be observed throughout other brain region (Fig. 3C–G). At E13.5, the *Rines* expression was detected in a thick layer facing the lateral ventricle, and the expression continued in the ventricular zone at E15.5 through E17.5 (Fig. 3C–G), but the stained layer was thinner at the later stages. In addition, Rines was expressed strongly by lens-forming cells (Fig. 3D). In the sagittal section of E17.5, the *Rines* expression was detected in the olfactory bulb, the ventricular layers facing both on the lateral ventricle and the fourth ventricle and weakly in the thalamus (Fig. 3F). A higher magnification of the cerebral cortex revealed that the *Rines* expression was restricted to the ventricular zone (Fig. 3G).

Rines has a protein-degradation activity dependent on proteasomal function

Because Rines was first found as a Zic2 binding protein in yeast, we performed GST pull-down experiments with the total cell extract from cells transfected with Flag-Rines and GST-fused Zic2 FL (full-length). The precipitates were immunoblotted to detect Flag-Rines (Fig. 4A). We obtained GST-fusion Zic2-bound Rines. To test if the interaction occurs between the purified proteins, we prepared a GST fusion protein containing the Rines fragment obtained from two-hybrid screening (two-hybrid binding region (TBR: 282–489), Fig. 4C) and used this fusion protein for GST pull-down experiments with purified Flag-2HA-Zic2 expressed in, and purified from, 293T cells (Fig. 4B). As a result, we could observe the interaction of GST-Rines-TBR with Flag-2HA-Zic2 (Fig. 4B). This result confirmed that Rines can directly interact with Zic2. Mapping of the Zic2 binding domain in TBR 282–489 revealed that both the basic coiled-coil domain and the RING finger domain were involved in the binding (Fig. 4C,D).

To test whether Rines can affect the protein amount of the interacting protein, 293T cells were co-transfected with Flag-Rines and HA-Zic2. We found that the amount of HA-Zic2 in the cell lysate was reduced only when Flag-Rines was co-transfected (Fig. 5A, Input lane2). We then speculated that Rines may be involved in proteasomal protein degradation, because a large number of proteins with the RING finger motif participated in proteasomal protein degradation. This idea led us to examine the HA-Zic2 protein amount in the cells treated with an inhibitor of proteasome function (MG132) or an inhibitor of lysosomal cysteine protease

© 2008 The Authors
Journal compilation © 2008 by the Molecular Biology Society of Japan/Blackwell Publishing Ltd.

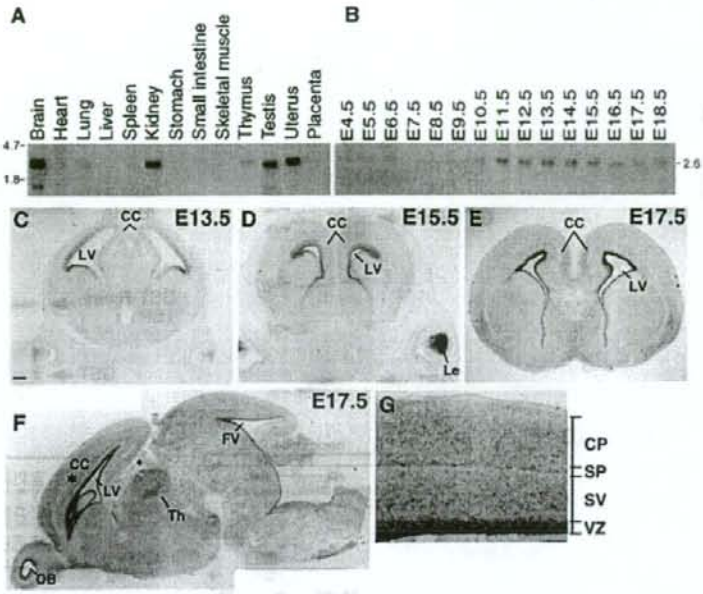

Figure 3 Expression of the Rines. (A–B) Northern blot analyses of a ^{32}P-labeled DNA probe of *Rines*. Each lane contains 20 μg of total RNA. (A) Tissue distribution of the *Rines* mRNA in adult mice. RNA derives from indicated organs of ICR mouse, age 6–10 weeks. (B) Developmental changes in the *Rines* mRNA expression in the mouse embryo from E4.5 to E18.5. (C–G) *in situ* hybridization analysis. *Rines* mRNA distribution is shown in brain sections from E13.5 (C), E15.5 (D), E17.5 (E, F, G) embryos. C–E show coronal sections and F and G show sagittal sections. (G) Higher magnification of the area indicated by asterisk in (F). *CC*, cerebral cortex; *CP*, cortical plate; *FV*, fourth ventricle; *Le*, lens; *LV*, lateral ventricle; *OB*, olfactory bulb; *SP*, subplate; *SV*, subventricular zone; *Th*, thalamus; *VZ*, ventricular zone. Scale bar, 200 μm.

Color

(E64). As shown in Fig. 5A, the HA-Zic2 in the input lysate decreased in the cells transfected with Flag-Rines was recovered in the cells with MG132 treatment. Similarly, the level of Flag-Rines itself was also increased by the treatment with MG132, but not with E64. In addition, the interaction of Flag-Rines and HA-Zic2 was observed in cells only when the cells were treated with MG132 but not with E64. These results suggest that the apparent absence of the Flag-Rines–HA-Zic2 complex in the cell lysate without MG132 may be due to the rapid degradation of this complex in the proteasome.

To further investigate whether Flag-Rines promotes the degradation of the interacting protein by the proteasome pathway, we examined the Zic2 amount by immunoblot analysis in cells using a series of proteasomal inhibitors or a calpain inhibitor (Fig. 5B). HA-Zic2 was co-transfected into cells with either Flag-Rines or Flag-tagged control vector. The result showed that the Rines-induced degradation of Zic2 was blocked in the presence of the all tested proteasome inhibitors including MG132, Epoxomicin, *clasto*-Lactacystin-β-lactone, Lactacystin and ALLN (Fig. 5B), but was not blocked even in the presence of the high concentration (1 μM) of the calpain inhibitor, Calpastatin peptide (IC50 = 20 nM, Eto *et al.* 1995) (Fig. 5B). These results confirm that Rines promotes the degradation of protein by the proteasome pathway.

To clarify whether or not the Flag-Rines-induced decrement of HA-Zic2 is due to the enhanced Zic2 degradation, we performed a cycloheximide chase experiment. HA-Zic2 was co-expressed in cells with either Flag-Rines or Flag-vector control. Cycloheximide was added 26 h after transfection to inhibit new protein synthesis, and cells were harvested at the indicated time points. The decay of HA-Zic2 was analyzed by immunoblotting. A clear effect on the stability of HA-Zic2 was observed in this cycloheximide chase experiment (Fig. 5C,D). In the presence of the Flag-Rines, the level of HA-Zic2 severely decreased at 4 and 6 h after cycloheximide addition, whereas this effect was not seen in the absence of Flag-Rines. These results indicate that Flag-Rines indeed shortens the half-life of HA-Zic2. We also observed a rapid decrement of Rines itself (Fig. 5C) in accord with the proteasomal degradation of Flag-Rines (Fig. 5A).

Rines can bind to a ubiquitin-conjugating E2 enzyme and shows ubiquitin-ligase activity

The RING finger motifs in RING-type E3s have been shown to serve as recruiting motifs for specific E2 ubiquitin-conjugating enzymes. It was considered that Rines is involved in the proteasomal machinery. To test whether Rines could recruit an E2-ubiquitin conjugating

© 2008 The Authors
Journal compilation © 2008 by the Molecular Biology Society of Japan/Blackwell Publishing Ltd.

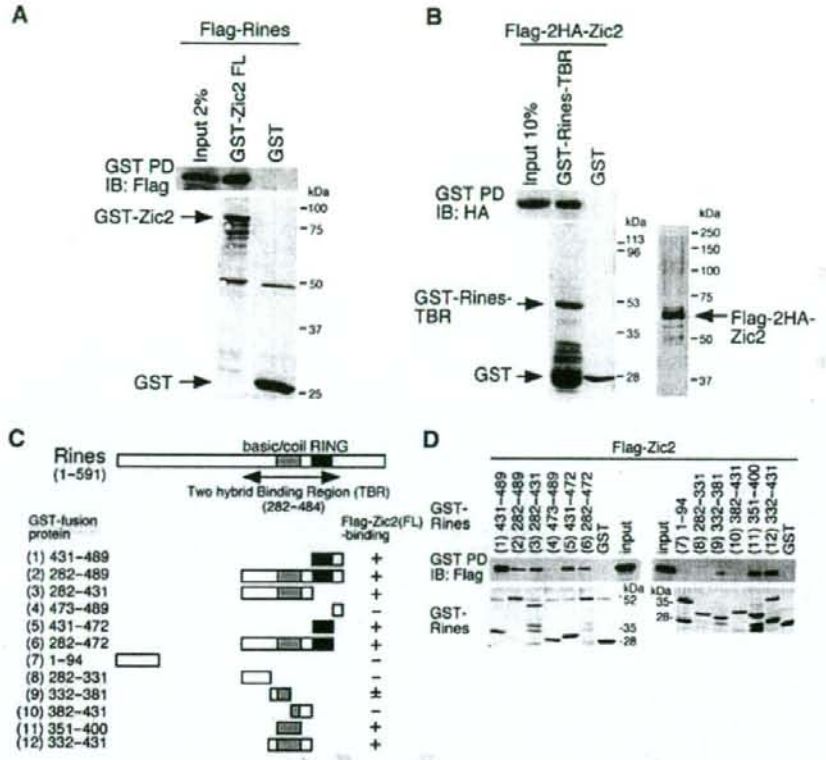

Figure 4 Zic2-binding activity of Rines. (A) Rines binds Zic2 *in vitro*. 293T cells were transfected with Flag-Rines, and the cell lysates containing equal amount of proteins were incubated with the GST-Zic2. The eluates from the glutathione sepharose beads were analyzed by immunoblotting with anti-Flag antibody (*upper panel*). GST-Zic2 was shown as amido black staining (*lower panel*). (B) Rines directly interact with Zic2. Flag-2HA-Zic2 expressed and purified from 293T cells was incubated with the GST-Rines-TBR (282–489) fusion protein or GST protein and GST pull-down assay was performed. Bound material was detected by immunoblotting using anti-HA antibody. GST-Rines-TBR fusion protein was shown as amido black staining (*lower left panel*). The input purified Flag-2HA-Zic2 was shown as silver staining (*lower right panel*). (C–D) Rines binds Zic2 in the basic coiled-coil domain and RING finger domain. (C, A) schematic representation of the Rines, its deletion mutants and the result of mapping of the Zic2-binding region in Rines. The various regions of the Rines were prepared as GST fusion proteins. The numbers refer to amino acids. D, GST pull-down assays. *Upper panel*, immunoblot using anti-Flag antibody; *lower panel*, amido black staining indicating GST-Rines deletion proteins.

enzyme, we performed a GST pull-down assay using GST-Rines-TBR, which contains the RING finger motif, and a set of the Myc-E2s (UbcH5a, H5b, H5 c, H6, H7 and H8) expressed in cells (Fig. 6A). As a result, GST-Rines-TBR associated with Myc-UbcH6, but not with Myc-UbcH5a, H5b, H5c, H7 or H8.

It is known that almost all known RING-type E3 ligases themselves are susceptible to be ubiquitinated (Fang & Weissman 2004). Overexpression of Myc- or Flag-Rines in 293T, NIH 3T3 and COS7 cells resulted in the formation of higher molecular weight bands that were recognized by immunoblot using anti-Myc or Flag antibodies (data not shown). We then examined whether Rines could be covalently modified by ubiquitin (Fig. 6B). An expression plasmid encoding a HA-ubiquitin was transfected into NIH 3T3 cells with or without plasmid for Flag-Rines, followed by immunoprecipitation with anti-Flag antibody. An immunoblot analysis of immunoprecipitates with anti-HA antibody showed a broad band with high molecular weight only when HA-ubiquitin and Flag-Rines were co-expressed. When the same samples were immunoblotted with anti-Flag antibody, the broad bands with high molecular weight appeared regardless of the presence of HA-ubiquitin. These results

© 2008 The Authors
Journal compilation © 2008 by the Molecular Biology Society of Japan/Blackwell Publishing Ltd.

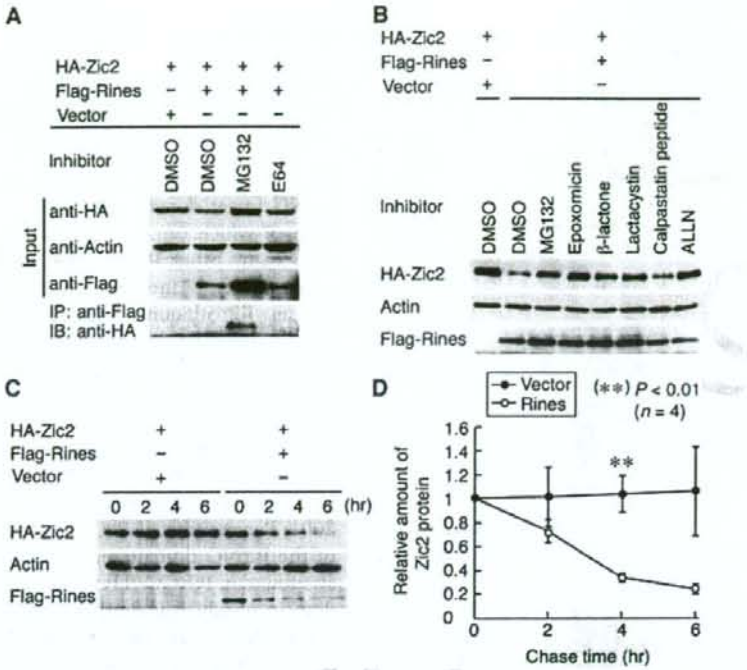

Figure 5 Proteasomal degradation-enhancing activity of Rines. (A) Co-immunoprecipitation of Rines with Zic2 from transfected cells. 293T cells were co-transfected with indicated vectors, and cultured with dimethylsulfoxide (DMSO), proteasome inhibitor MG132 (20 μM), or lysosomal protease inhibitor E64 (50 μM). An equal amount of protein from each cell lysate was subjected to immunoprecipitation and immunoblotting using the antibodies indicated (*top panel*). Expression analysis of the HA-, Flag-tagged gene products and actin protein (as internal control) was done by immunoblotting of the cell extracts (*bottom three panels*). The protein ratio used for immunoprecipitation and immunoblotting lanes was 40 : 1. (B) The effects of Rines on Zic2 degradation were blocked by the proteasome inhibitors but not the calpain inhibitor. NIH 3T3 cells were co-transfected with indicated vectors, and were treated with the proteasome inhibitor, MG132 (10 μM), Epoxomicin (10 μM), *clasto*-Lactacystin-β-lactone (10 μM), Lactacystin (20 μM), ALLN (25 μM), the calpain inhibitor, Calpastatine peptide (1 μM) or vehicle (DMSO). The cell lysates were analyzed by immunoblotting. (C–D) Rines accelerates Zic2 turnover. (C) NIH 3T3 cells were transfected with indicated vectors and cultured with cycloheximide, The cell lysates prepared at 0, 2, 4 and 6 h after cycloheximide treatment were analyzed by immunoblotting with anti-HA, anti-Flag or anti-actin antibodies. (D) Relative amount of Zic2. The Zic2 amounts have been normalized to actin so that the value for the amounts at 0 h equals 1.0. The plots indicate means of four independent analyses. Error bars represent standard error. Asterisk denotes statistical significance in the Zic2 amount between the Flag-Rines-transfected and the control vector-transfected cell lysates. **, $P < 0.01$, $n = 4$, by Student's *t*-test.

indicate that Flag-Rines is heavily ubiquitinated and Flag-Rines can be modified with endogenous ubiquitin as well as exogenous ubiquitin.

Next, we tested whether Rines has an ubiquitin ligase activity (Fig. 7A). Flag-Zic2 was co-transfected into NIH 3T3 cells along with HA-tagged ubiquitin in the absence or presence of a plasmid with Myc-tagged Rines. Cell lysates were subjected to immunoprecipitation with an anti-Flag antibody, followed by immunoblotting with an anti-HA antibody to detect ubiquitin-conjugated Zic2. A broad band with high molecular weight was more enhanced in the presence of Myc-Rines than in its absence. Accordingly, the ubiquitination of endogenous Zic2 was enhanced by Myc-Rines in rat neural stem cell line MNS70 cells (Fig. 7B). These results indicate that Rines can promote the polyubiquitination of the interacting protein. Furthermore, deletion of the RING finger motif abolished the ability of Rines to promote the ubiquitination of endogenous Zic2 – the ability integral Rines possesses (Fig. 7B). Because the RING finger motif is suggested to be essential for the enzymatic activity of RING-type E3 ubiquitin ligase (Joazeiro & Weissman

© 2008 The Authors
Journal compilation © 2008 by the Molecular Biology Society of Japan/Blackwell Publishing Ltd.